Science
AAAS

Supplementary Materials for

Tunable light-induced dipole-dipole interaction between optically levitated nanoparticles

Jakob Rieser *et al*.

Corresponding authors: Benjamin A. Stickler, benjamin.stickler@uni-due.de; Uroš Delić, uros.delic@univie.ac.at

Science **377**, 987 (2022)
DOI: 10.1126/science.abp9941

The PDF file includes:

Materials and Methods
Figs. S1 to S3
Table S1
References

Materials and Methods

Theory basics

At this point we will sketch the derivation of the equations of motion and the coupling constants. The force on a dipole is given by the gradient of the scalar product of its dipole moment with the incident electric field, where the gradient only acts on the electric field, treating the dipole moment as a constant. We can express the dipole moments inside of a j-th dielectric particle via the particles polarizability $\alpha_j = \varepsilon_0 V_j \chi$ and the drive (trapping) field $\mathbf{E}_0(\mathbf{r})$, with the particle volume V_j and $\chi = 3(\varepsilon - 1)/(\varepsilon + 2)$ with the permittivity ε. The incident field at the position $\mathbf{r}_j$ away from a particle is a sum of $\mathbf{E}_0(\mathbf{r})$ and the scattering fields of all other particles, which can be expressed by the Green's tensor $\mathbf{G}(\mathbf{r})$ of the transverse Helmholtz equation:

$$\mathbf{G}(\mathbf{r}) = \frac{e^{ikr}}{4\pi}\left[\frac{3\mathbf{r}\otimes\mathbf{r} - r^2}{r^5}(1 - ikr) + k^2\frac{r^2 - \mathbf{r}\otimes\mathbf{r}}{r^3}\right], \tag{S1}$$

with $r = |\mathbf{r}|$ and where we omitted the unity matrix for simplicity.

By expanding the force to the second order in the particle volume, one can identify three contributions to the total force acting on one particle. The first is a sum of the well-known gradient force and the non-conservative radiation pressure originating only from the trapping field. The second contribution comes from the scattering fields of the other particles acting on the dipole moment due to the laser field, while the third contribution can be interpreted as the laser acting on the dipole moment induced by the scattering fields of the other particles. The second and third contribution together condense in what is called the optical binding force:

$$\mathbf{F}_j^{\mathrm{bind}} = \nabla_j \mathrm{Re}\left[\sum_{j'\neq j}\frac{\alpha_j\alpha_{j'}}{2\varepsilon_0}\mathbf{E}_0^*(\mathbf{r}_j)\cdot\mathbf{G}(\mathbf{r}_j - \mathbf{r}_{j'})\mathbf{E}_0(\mathbf{r}_{j'})\right], \tag{S2}$$

with the nabla operator ∇_j acting on the coordinate $\mathbf{r}_j$. Expanding the forces to the third order in the particle volume would add the gradient force of scattering fields alone, as well as the interaction of the trapping field with the second order scattering fields. However, we will neglect these higher order terms ($\sim \mathcal{O}(V^3)$) in this work.

In the far-field (interparticle distance $\gg 1/k$) the Green function in Eq. S2 can be approximated by its far-field expression by keeping only the last term in equation Eq. S1. If the particles are deeply trapped in their respective Gaussian beam traps, the electric fields in Eq. S2 can be treated locally as Gaussian beams traveling in positive z-direction as $\mathbf{E}(\mathbf{r}_{1,2}) \approx \mathbf{E}_{1,2} \exp[i(k - 1/z_\mathrm{R})z_{1,2} + i\phi_{1,2}]$, with the Rayleigh range z_R, the local field strengths $\mathbf{E}_{1,2}$ and the local phases in the focal plane $\phi_{1,2}$. The gradient in Eq. S2 acts to leading order only on the exponential function in Eq. S1 and the phases of the tweezer fields. If both tweezers have identical polarization, the optical binding forces on two particles can be written as

$$\mathbf{F}_{1,2}^\mathrm{bind} \approx \frac{\alpha_1 \alpha_2 k^2}{8\pi\varepsilon_0 d} \cos^2\Theta \sin(kd \mp \Delta\phi) \left[\pm k\mathbf{n} + (k - 1/z_\mathrm{R})\mathbf{e}_z\right], \tag{S3}$$

where $d = |\mathbf{r}_1 - \mathbf{r}_2|$ denotes the particle distance, $\pi/2 - \Theta$ is the angle between the laser polarization and the particle connecting axis, $\Delta\phi = \Delta\phi_0 + (k - 1/z_\mathrm{R})(z_1 - z_2)$ the local phase difference of the beams with $\Delta\phi_0 = \phi_1 - \phi_2$ the phase difference in the focal plane, and $\mathbf{n} = (\mathbf{r}_1 - \mathbf{r}_2)/d$ the unity vector pointing from particle 1 to particle 2.

The coupling rates can be derived by expanding the optical binding forces around the equilibrium positions of the two particles, as determined by the gradient force of the trapping field. Along the optical axis, the dominant contribution to the coupling is due to the dependence of $\Delta\phi$ on $z_{1,2}$. If the particles have trapping frequencies $\Omega_{1,2}$ and an identical mass m, the linearized dynamics along the optical axis with particle coordinates $z_{1,2}$ is then, to leading order

in the tweezer separation d_0, determined by the coupling constants k_1 and k_2,

$$\begin{aligned} m\ddot{z}_1 &= -\left(m\Omega_1^2 + k_1 + k_2\right) z_1 + (k_1 + k_2) z_2 \\ m\ddot{z}_2 &= -\left(m\Omega_2^2 + k_1 - k_2\right) z_2 + (k_1 - k_2) z_1. \end{aligned} \tag{S4}$$

The coupling constant k_1 describes the conservative part of the optical binding forces, while k_2 describes a non-conservative interaction, as indicated by the opposite sign in the equations of motion. They depend on the relative local phase $\Delta\phi_0 = \phi_1 - \phi_2$ and the tweezer separation d_0 as $k_1 = G\cos(kd_0)\cos(\Delta\phi_0)/kd_0$ and $k_2 = G\sin(kd_0)\sin(\Delta\phi_0)/kd_0$. Constant $G = \alpha^2 k^3 (k - 1/z_R)^2 \sqrt{P_1 P_2}/(2cw_0^2\pi^2\varepsilon_0^2)$ is a positive function of the particle polarizability α and optical powers $P_{1,2}$, where w_0 is the trap waist, ε_0 is the vacuum permittivity and c is the speed of light. The distance d_0 and the relative tweezer phase $\Delta\phi_0$ allow tuning between purely conservative and non-conservative interactions.

The non-conservative contribution to optical binding emerges from the radiation pressure induced by the scattered fields, which constantly pumps energy into the system, thus it can't be derived from a Hamiltonian. This is also observed with curl-forces (*36*), in ro-translational oscillators (*16,37*) or for binding of particles of different sizes (*38–40*). The equations of motion along the x and y axes follow the same form.

Eigenfrequencies of the coupled system

We diagonalize Eqs. S4 in order to obtain the eigenfrequencies of the normal modes for arbitrary intrinsic mechanical frequencies $\Omega_1 = \Omega\sqrt{1+\eta}$ and $\Omega_2 = \Omega\sqrt{1-\eta}$:

$$\Omega_\pm^2 = \frac{1}{2}\left(\Omega_2^2 + \Omega_1^2 + 2k_1/m \mp \sqrt{(\Omega_2^2 - \Omega_1^2)^2 + 4(k_1/m)^2 - 4(\Omega_2^2 - \Omega_1^2)k_2/m}\right) \tag{S5a}$$

$$= \Omega^2 + k_1/m \mp \sqrt{\Omega^4\,\eta^2 + 2\Omega^2\eta k_2/m + (k_1/m)^2}, \tag{S5b}$$

where η is the control parameter and Ω is the frequency of both modes for $\eta = 0$ and no interaction. The splitting is minimal for $\Omega_2^2 - \Omega_1^2 = 2k_2/m$, which is reached for $\eta_\mathrm{m} = -k_2/(m\Omega^2)$.

For small k_1, $k_2 \ll m\Omega^2$ the eigenfrequencies at the avoided crossing are:

$$\Omega_\pm(\eta_m) = \sqrt{\Omega^2 + k_1/m \mp \sqrt{k_1^2 - k_2^2}/m} \approx \Omega + \frac{k_1}{2m\Omega} \mp \frac{\sqrt{k_1^2 - k_2^2}}{2m\Omega}, \tag{S6}$$

with the splitting of:

$$\Omega_-(\eta_m) - \Omega_+(\eta_m) \approx \frac{\sqrt{k_1^2 - k_2^2}}{m\Omega}. \tag{S7}$$

The conservative interaction has to be larger than the non-conservative interaction $k_1^2 > k_2^2$ in order to observe an avoided crossing. In the case of purely conservative interaction ($k_2 \equiv 0$) the splitting is minimal for $\eta_m \equiv 0$:

$$\begin{aligned} \Omega_\pm = \sqrt{\Omega^2 + (k_1 \mp |k_1|)/m} \quad &\Rightarrow \quad \Omega_+ = \Omega, \Omega_- \approx \Omega + \frac{k_1}{m\Omega} \\ \Omega_- - \Omega_+ \quad &\approx \quad \frac{k_1}{m\Omega} = 2g. \end{aligned} \tag{S8}$$

In the case of $k_1^2 < k_2^2$ the modes become degenerate for a range of values of $\eta = [\eta_1, \eta_2]$, where:

$$\eta_{1(2)} = \min(\max)\left\{ -\frac{k_2}{m\Omega^2} \pm \sqrt{\left(\frac{k_2}{m\Omega^2}\right)^2 - \left(\frac{k_1}{m\Omega^2}\right)^2} \right\} \tag{S9}$$

Interaction suppression by polarization

The radiated electric field for an arbitrary polarization angle Θ consists of a radial and an azimuthal contribution:

$$\begin{aligned} E_R(R) &= -E_0 \frac{\alpha k^2 \sin\Theta}{4\pi\varepsilon_0 R} e^{ikR} \left(\frac{2}{k^2R^2} - \frac{2i}{kR} \right) \\ E_\varphi(R) &= -E_0 \frac{\alpha k^2 \cos\Theta}{4\pi\varepsilon_0 R} e^{ikR} \left(\frac{1}{k^2R^2} - \frac{i}{kR} - 1 \right). \end{aligned} \tag{S10}$$

If the light is polarized along the x axis ($\Theta = 90°$), the azimuthal component of the radiated field disappears $E_\varphi \equiv 0$. However, the near-field radial component E_R yields the following conservative coupling rate:

$$g_{\text{near}}(d_0, \Delta\phi_0 = 0) = \frac{G}{2\Omega} \left(-\frac{2}{k^3 d_0^3} \cos(kd_0) + \frac{2}{k^2 d_0^2} \sin(kd_0) \right). \tag{S11}$$

For $d_0 \sim 3\lambda$ the coupling rate is a factor of $2/(36\pi^2) \approx 5.6 \times 10^{-3}$ of the coupling rate for $\Theta = 0°$.

Electrostatic interaction

Electrostatic interaction between dielectric objects is purely conservative with the interaction energy:

$$H_C = \frac{1}{4\pi\varepsilon_0} \frac{q_1 q_2}{\sqrt{(d_0 + x_1 - x_2)^2 + (y_1 - y_2)^2 + (z_1 - z_2)^2}}, \tag{S12}$$

where q_1 and q_2 are particle charges, d_0 is the trap separation and particle motions $x_{1,2}$, $y_{1,2}$ and $z_{1,2}$. We expand the Hamiltonian to the second order in $z_{1,2}$ and obtain:

$$H_C = \frac{1}{4\pi\varepsilon_0} \frac{q_1 q_2}{d_0} \left(1 - \frac{(z_1 - z_2)^2}{2d_0^2}\right) \equiv \frac{k_1}{2}(z_1^2 + z_2^2) - k_1 z_1 z_2, \tag{S13}$$

where we have defined $k_1 = -\frac{q_1 q_2}{4\pi\varepsilon_0 m} \frac{1}{d_0^3}$ in analogy to the conservative optical interaction. The coupling rate due to the electrostatic interaction is given by:

$$g_C = \frac{k_1}{2m\Omega'} = -\frac{q_1 q_2}{8\pi\varepsilon_0 m\Omega'} \frac{1}{d_0^3}, \tag{S14}$$

where $\Omega' = \sqrt{\Omega^2 - \frac{q_1 q_2}{4\pi\varepsilon_0 m d_0^3}}$ is the modified mechanical frequency due to the electrostatic interaction.

Experimental setup

The experimental setup is shown in Fig. S1. The trapping beam ($\lambda = 1064$ nm, Keopsys fiber amplifier seeded by a Mephisto laser) is expanded to a diameter of 8.7 mm in order to overfill the apertures of the spatial light modulator (SLM, Meadowlark Inc. 512x512 pixels) and the microscope objective. We imprint a phase profile with the SLM into the trapping beam that transforms into an amplitude profile in the Fourier plane of the trapping optics. The phase profile is calibrated to compensate for aberrations, nonlinearities of the SLM response and non-flatness of the SLM surface. Inset of Fig. S1 shows the phase profile used to generate two traps

spaced by 3.4 μm. This phase profile is imaged onto the trapping optics using a 1:1 telescope set in a 4f configuration (focal length of lenses 300 mm). The trap is then generated using a microscope objective (CFU TU Plan Fluor EPI 50x, Nikon Corp., NA$= 0.8$, WD $=$ 1mm), focusing the beam to two traps of waist $\approx 730nm$. The total power used in front of the vacuum chamber is ≈ 1.2 W. We maintain a stable pressure of $p \approx 1.5$ mbar in the vacuum chamber, at which a single particle is in a thermal equilibrium with the environment.

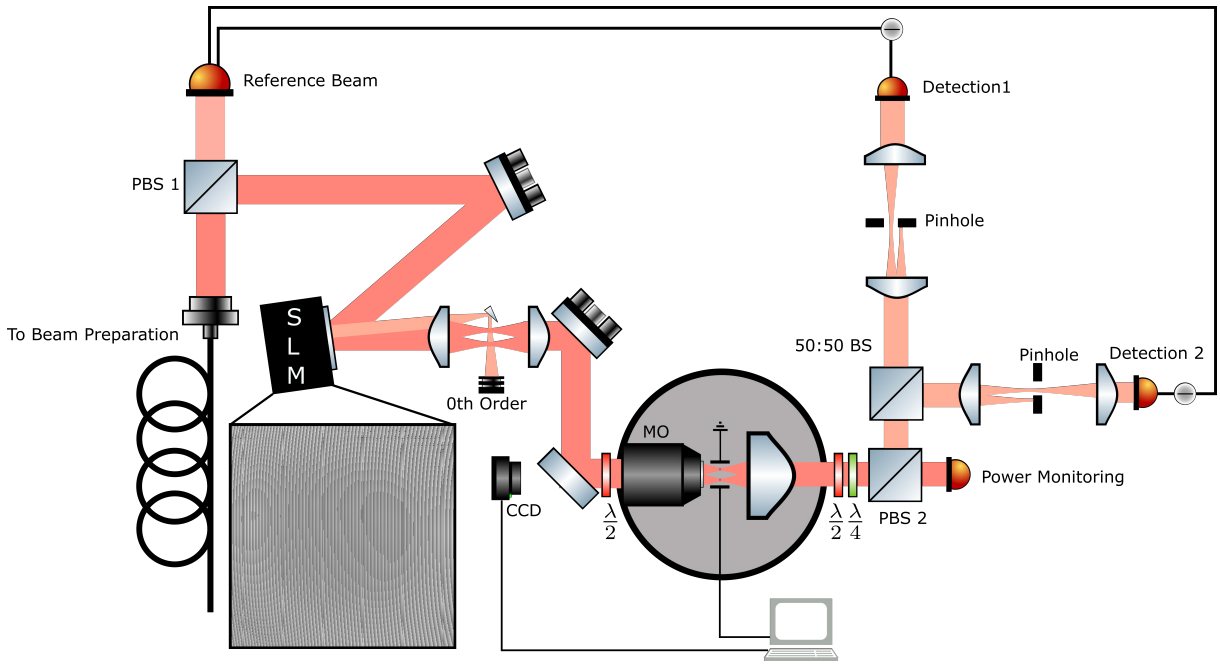

Figure S1: Setup for generating multiple traps using a spatial light modulator. 1064 nm laser light, with a diameter of 8.7mm, is reflected on a Spatial Light Modulator (SLM Meadowlark Inc.) where a phase profile is imprinted. In the Fourier plane of the trapping objective the phase profile is translated into an amplitude profile with correct imaging being ensured via a 4f configuration using a 1:1 telescope. The light is recollimated and split for detection, with the traps being selected using movable pin holes in 1:1 telescopes.

A pair of electrodes mounted on a 3D piezo stage (MX25, Mechonics Inc.) is placed around the beam focus, with a spacing of $D_c = (230 \pm 15)$ μm. The light is recollimated using an aspheric lens (C660TME-C, Thorlabs) and split at a polarization beamsplitter (PBS2) for power monitoring. The reflected arm is split with a $50:50$ beamsplitter. We mount a pinhole

on a translation stage in the focus of a 1:1 telescope ($f = 125$ mm) in each of the beamsplitter outputs, which we use to select individual laser beams in order to separate the detection. In each arm the trapping beam goes onto one photodiode of a balanced photodetector (PDB425C, Thorlabs), while the reference beam of equal power (taken from PBS1) is focused onto the other photodiode in order to suppress the intensity noise. We acquire 2 seconds of data at a sampling rate of 2.5 MSa/s with an oscilloscope (PicoScope 5444D).

Charge calibration

In order to estimate the magnitude of the electrostatic interaction between the particles, we performed charge calibration for each particle used in the experimental runs. We increase the trap separation to approximately 18 μm in order to minimize all interactions and cross-talk in the detection. We subsequently apply a sinusoidal voltage ($F_d(t) = F_0 \sin(\Omega_d t)$) to the electrodes set along the x axis, with the driving frequency Ω_d close to the mechanical frequencies along the x axis Ω_x. We measure the particle displacement as a function of the driving frequency (*7*):

$$\langle x_d^2 \rangle = \frac{\langle F_d^2 \rangle}{m^2(\Omega_x^2 - \Omega_d^2)^2} \tag{S15}$$

Here, $\langle \cdot \rangle$ is the time average, $\langle F_d^2 \rangle = F_0^2/2$ is the applied half-amplitude force, $m = (7.0 \pm 0.7)$ fg is the particle mass, Ω_x is the trap frequency (in rad/s) along the x axis, Ω_d is the drive frequency (in rad/s).

Assuming a model for a massive point charge in a parallel-plate capacitor, we get $F_0 = \frac{qV}{D_c}$ where $q = Ne$ is the particle charge, V is the applied voltage and $D_c = (230 \pm 15)$ μm is the distance between the electrodes. We can express Eq. S15 in terms of the number of charges to get:

$$N = \frac{\sqrt{2} m D_c}{eV} \left|\Omega_x^2 - \Omega_d^2\right| \sqrt{\langle x_d^2 \rangle} \tag{S16}$$

After a position-displacement calibration (*41*), we extract $\langle x_d^2 \rangle$ by integrating over the drive

frequency in the spectrum. Table S1 lists the number of charges for each particle used in the main text.

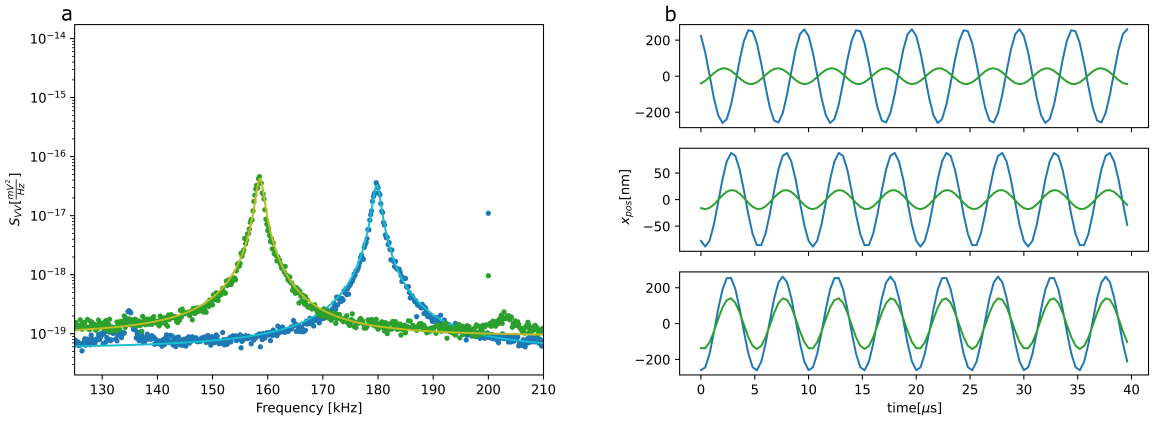

Figure S2: a) Example spectra with the drive frequency $\Omega_d = 2\pi \times 200$ kHz. The mechanical frequencies are set to be different in order to check that we have independent readout of the particles. b) Time trace of the driven particle motion at the drive frequency. The phase between the particles is indicative of the sign of the charges. Equal and opposite sign of charges is reflected in the in-phase or out-of-phase response to the drive, respectively.

Figure in the main text	$\lvert N_1 \rvert$	$\lvert N_2 \rvert$	sign($N_1 N_2$)	g_C/Ω'
3a	23 ± 5	5 ± 2	-1	$(4.6 \pm 2.1) \times 10^{-4}$
3b	3 ± 1	1 ± 1	1	$-(1.2 \pm 1.3) \times 10^{-5}$
4c	1 ± 1	0 ± 1	n.a.	$(0 \pm 4) \times 10^{-6}$
4d	110 ± 24	96 ± 21	1	-0.047 ± 0.015

Table S1: Results of the charge calibrations performed on 4 sets of particles. N_1 and N_2 are the number of elementary charges on the particles. Each row represents a set of particles used for measurements in the main text. We provide the coupling rate due to the electrostatic interaction at a distance of $3.2\ \mu$m $\approx 3\lambda$ and for the mechanical frequency $\Omega = 2\pi \times 50$ kHz.

Interaction model used for fitting

We correct for aberrations *in situ* with the SLM, however the trapping field still has the shape of an Airy function in the focus due to the high numerical aperture of the microscope objective. This leads to a small overlap of the trapping fields at distances larger than the trap waist,

therefore we are unable to separate the trapping fields in the description of the total interaction. This leads to a "self-interference" effect, where for example at the position of particle 2 the scattered field of particle 1 interferes with the tail of the trapping field for particle 1 (*14*). We model this with a standing wave in the focal plane with a relative electric field magnitude A. Already a weak tail of the trapping potential can have a large impact as it becomes comparable to the magnitude of the dipole radiation. This effect leads to a slight modification of the trap positions.

Furthermore, the radiation pressure of the scattered fields displaces the particles from the desired trap positions. The actual distance between the particles is smaller (larger) in the presence of an attractive (repulsive) force. This is confirmed when we compare coupling rates obtained for $\Delta\phi_0 = 0$ and $\Delta\phi_0 = \pi$ in Fig. 3a in the main text; the period between the zero crossings of the coupling rate is larger for positive coupling rates, which is a result of the displacement by the optical force.

We include both effects in the model of the dipole-dipole interaction and find an excellent fit between the model and the experimental data for distances larger than ~ 2.4 μm in Figure 3a in the main text. We point out that at smaller trap separations we neglect several features of the trap potential and the near-field optical interaction, as well as the (small) effect of the aerodynamic coupling. In future experiments at closer trap separations we will have to investigate the trap potential shape, as well as include the dipole radiation component $\propto d_0^{-2}$ which is non-negligible at trap separations $d_0 \sim \lambda$.

Normal mode splitting of the x and y motions

In the main text we have presented the results obtained only for the motion along the optical axes (z axes). However, standard optical binding interaction exists for all three directions of the particle motion due to the modification of the interparticle distance $d^2 = (d_0 + x_1 - x_2)^2 +$

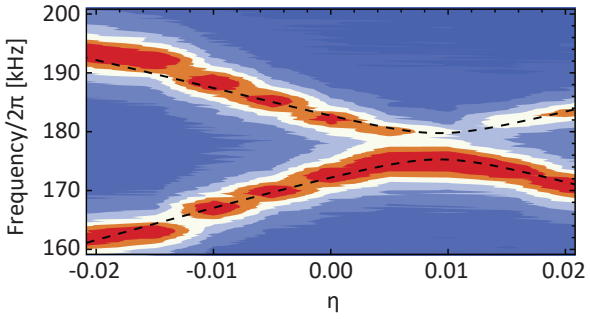

Figure S3: Normal mode splitting of the x motion due to the dipole-dipole interaction between two particles at a distance $d_0 \approx 2.2$ μm.

$(y_1 - y_2)^2 + (z_1 - z_2)^2$. The coupling rate between the x motions has the following form: $g_x \sim G/(2\Omega_x k d_0)$. We observe an avoided crossing between the x motions at a distance $d_0 \approx 2.2$ μm (Fig. S3). We extract the coupling rate of $g_x/\Omega_x' = 0.013 \pm 0.002$, which is significantly smaller than the coupling rate between the z motions from the main text as expected. The coupling rate g_x/Ω_x' scales $\propto \Omega_x^{-2}$, thus the higher mechanical frequency by a factor of $\Omega_x/\Omega \approx 4$ yields a smaller ratio g_x/Ω_x by a factor of ~ 16 in comparison to g/Ω, which fits to the measured value of $g/\Omega' \approx 0.186$ from the main text. We are unable to observe the avoided crossing between the y motions as the coupling rate is smaller than the mechanical damping.

References and Notes

1. A. Ashkin, J. M. Dziedzic, J. E. Bjorkholm, S. Chu, Observation of a single-beam gradient force optical trap for dielectric particles. *Opt. Lett.* **11**, 288 (1986). doi:10.1364/OL.11.000288 Medline

2. D. R. Leibrandt, J. Labaziewicz, V. Vuletić, I. L. Chuang, Cavity sideband cooling of a single trapped ion. *Phys. Rev. Lett.* **103**, 103001 (2009). doi:10.1103/PhysRevLett.103.103001 Medline

3. M. Hosseini, Y. Duan, K. M. Beck, Y.-T. Chen, V. Vuletić, Cavity Cooling of Many Atoms. *Phys. Rev. Lett.* **118**, 183601 (2017). doi:10.1103/PhysRevLett.118.183601 Medline

4. U. Delić, M. Reisenbauer, D. Grass, N. Kiesel, V. Vuletić, M. Aspelmeyer, Cavity Cooling of a Levitated Nanosphere by Coherent Scattering. *Phys. Rev. Lett.* **122**, 123602 (2019). doi:10.1103/PhysRevLett.122.123602 Medline

5. D. Windey, C. Gonzalez-Ballestero, P. Maurer, L. Novotny, O. Romero-Isart, R. Reimann, Cavity-Based 3D Cooling of a Levitated Nanoparticle via Coherent Scattering. *Phys. Rev. Lett.* **122**, 123601 (2019). doi:10.1103/PhysRevLett.122.123601 Medline

6. U. Delić, M. Reisenbauer, K. Dare, D. Grass, V. Vuletić, N. Kiesel, M. Aspelmeyer, Cooling of a levitated nanoparticle to the motional quantum ground state. *Science* **367**, 892–895 (2020). doi:10.1126/science.aba3993 Medline

7. L. Magrini, P. Rosenzweig, C. Bach, A. Deutschmann-Olek, S. G. Hofer, S. Hong, N. Kiesel, A. Kugi, M. Aspelmeyer, Real-time optimal quantum control of mechanical motion at room temperature. *Nature* **595**, 373–377 (2021). doi:10.1038/s41586-021-03602-3 Medline

8. F. Tebbenjohanns, M. L. Mattana, M. Rossi, M. Frimmer, L. Novotny, Quantum control of a nanoparticle optically levitated in cryogenic free space. *Nature* **595**, 378–382 (2021). doi:10.1038/s41586-021-03617-w Medline

9. K. Dholakia, P. Zemánek, *Colloquium*: Gripped by light: Optical binding. *Rev. Mod. Phys.* **82**, 1767–1791 (2010). doi:10.1103/RevModPhys.82.1767

10. M. M. Burns, J.-M. Fournier, J. A. Golovchenko, Optical binding. *Phys. Rev. Lett.* **63**, 1233–1236 (1989). doi:10.1103/PhysRevLett.63.1233 Medline

11. W. Singer, M. Frick, S. Bernet, M. Ritsch-Marte, Self-organized array of regularly spaced microbeads in a fiber-optical trap. *J. Opt. Soc. Am. B* **20**, 1568 (2003). doi:10.1364/JOSAB.20.001568

12. S. A. Tatarkova, A. E. Carruthers, K. Dholakia, One-dimensional optically bound arrays of microscopic particles. *Phys. Rev. Lett.* **89**, 283901 (2002). doi:10.1103/PhysRevLett.89.283901 Medline

13. S. Mohanty, J. Andrews, P. Gupta, Optical binding between dielectric particles. *Opt. Express* **12**, 2746–2753 (2004). doi:10.1364/OPEX.12.002746 Medline

14. M.-T. Wei, J. Ng, C. T. Chan, H. D. Ou-Yang, Lateral optical binding between two colloidal particles. *Sci. Rep.* **6**, 38883 (2016). doi:10.1038/srep38883 Medline

15. D. S. Bykov, S. Xie, R. Zeltner, A. Machnev, G. K. L. Wong, T. G. Euser, P. S. J. Russell, Long-range optical trapping and binding of microparticles in hollow-core photonic crystal fibre. *Light Sci. Appl.* **7**, 22 (2018). doi:10.1038/s41377-018-0015-z Medline

16. Y. Arita, E. M. Wright, K. Dholakia, Optical binding of two cooled micro-gyroscopes levitated in vacuum. *Optica* **5**, 910 (2018). doi:10.1364/OPTICA.5.000910

17. J. Damková, L. Chvátal, J. Ježek, J. Oulehla, O. Brzobohatý, P. Zemánek, Enhancement of the 'tractor-beam' pulling force on an optically bound structure. *Light Sci. Appl.* **7**, 17135 (2018). doi:10.1038/lsa.2017.135 Medline

18. V. Svak, J. Flajšmanová, L. Chvátal, M. Šiler, A. Jonáš, J. Ježek, S. H. Simpson, P. Zemánek, O. Brzobohatý, Stochastic dynamics of optically bound matter levitated in vacuum. *Optica* **8**, 220 (2021). doi:10.1364/OPTICA.404851

19. Y. Zhang, C. Gu, A. M. Schwartzberg, S. Chen, J. Z. Zhang, Optical trapping and light-induced agglomeration of gold nanoparticle aggregates. *Phys. Rev. B* **73**, 165405 (2006). doi:10.1103/PhysRevB.73.165405

20. F. Svedberg, Z. Li, H. Xu, M. Käll, Creating hot nanoparticle pairs for surface-enhanced Raman spectroscopy through optical manipulation. *Nano Lett.* **6**, 2639–2641 (2006). doi:10.1021/nl062101m Medline

21. V. Demergis, E.-L. Florin, Ultrastrong optical binding of metallic nanoparticles. *Nano Lett.* **12**, 5756–5760 (2012). doi:10.1021/nl303035p Medline

22. W. Lechner, S. J. M. Habraken, N. Kiesel, M. Aspelmeyer, P. Zoller, Cavity optomechanics of levitated nanodumbbells: Nonequilibrium phases and self-assembly. *Phys. Rev. Lett.* **110**, 143604 (2013). doi:10.1103/PhysRevLett.110.143604 Medline

23. D. Holzmann, M. Sonnleitner, H. Ritsch, Self-ordering and collective dynamics of transversely illuminated point-scatterers in a 1D trap. *Eur. Phys. J. D* **68**, 352 (2014). doi:10.1140/epjd/e2014-50692-2

24. S. Liu, Z. Yin, T. Li, Prethermalization and Nonreciprocal Phonon Transport in a Levitated Optomechanical Array. *Adv. Quantum Technol.* **3**, 1900099 (2020). doi:10.1002/qute.201900099

25. S. Ebadi, T. T. Wang, H. Levine, A. Keesling, G. Semeghini, A. Omran, D. Bluvstein, R. Samajdar, H. Pichler, W. W. Ho, S. Choi, S. Sachdev, M. Greiner, V. Vuletić, M. D. Lukin, Quantum phases of matter on a 256-atom programmable quantum simulator. *Nature* **595**, 227–232 (2021). doi:10.1038/s41586-021-03582-4 Medline

26. P. Scholl, M. Schuler, H. J. Williams, A. A. Eberharter, D. Barredo, K.-N. Schymik, V. Lienhard, L.-P. Henry, T. C. Lang, T. Lahaye, A. M. Läuchli, A. Browaeys, Quantum simulation of 2D antiferromagnets with hundreds of Rydberg atoms. *Nature* **595**, 233–238 (2021). doi:10.1038/s41586-021-03585-1 Medline

27. V. Peano, C. Brendel, M. Schmidt, F. Marquardt, Topological Phases of Sound and Light. *Phys. Rev. X* **5**, 031011 (2015). doi:10.1103/PhysRevX.5.031011

28. N. Goldman, J. C. Budich, P. Zoller, Topological quantum matter with ultracold gases in optical lattices. *Nat. Phys.* **12**, 639–645 (2016). doi:10.1038/nphys3803

29. See the supplementary materials.

30. J. K. Asbóth, P. Domokos, H. Ritsch, Correlated motion of two atoms trapped in a single-mode cavity field. *Phys. Rev. A* **70**, 013414 (2004). doi:10.1103/PhysRevA.70.013414

31. M. Ludwig, F. Marquardt, Quantum many-body dynamics in optomechanical arrays. *Phys. Rev. Lett.* **111**, 073603 (2013). doi:10.1103/PhysRevLett.111.073603 Medline

32. G. Heinrich, M. Ludwig, J. Qian, B. Kubala, F. Marquardt, Collective dynamics in optomechanical arrays. *Phys. Rev. Lett.* **107**, 043603 (2011). doi:10.1103/PhysRevLett.107.043603 Medline

33. D. Holzmann, M. Sonnleitner, H. Ritsch, A Versatile Quantum Simulator for Coupled Oscillators Using a 1D Chain of Atoms Trapped near an Optical Nanofiber. *Photonics* **8**, 228 (2021). doi:10.3390/photonics8060228

34. A. McDonald, A. A. Clerk, Exponentially-enhanced quantum sensing with non-Hermitian lattice dynamics. *Nat. Commun.* **11**, 5382 (2020). doi:10.1038/s41467-020-19090-4 Medline

35. P. Domokos, H. Ritsch, Collective cooling and self-organization of atoms in a cavity. *Phys. Rev. Lett.* **89**, 253003 (2002). doi:10.1103/PhysRevLett.89.253003 Medline

36. M. V. Berry, P. Shukla, Physical curl forces: Dipole dynamics near optical vortices. *J. Phys. A Math. Theor.* **46**, 422001 (2013). doi:10.1088/1751-8113/46/42/422001

37. S. H. Simpson, P. Zemánek, O. M. Maragò, P. H. Jones, S. Hanna, Optical Binding of Nanowires. *Nano Lett.* **17**, 3485–3492 (2017). doi:10.1021/acs.nanolett.7b00494 Medline

38. V. Karásek, M. Šiler, O. Brzobohatý, P. Zemánek, Dynamics of an optically bound structure made of particles of unequal sizes. *Opt. Lett.* **42**, 1436–1439 (2017). doi:10.1364/OL.42.001436 Medline

39. S. Sukhov, A. Shalin, D. Haefner, A. Dogariu, *Actio et reactio* in optical binding. *Opt. Express* **23**, 247–252 (2015). doi:10.1364/OE.23.000247 Medline

40. L. Chvátal, O. Brzobohatý, P. Zemánek, Binding of a pair of Au nanoparticles in a wide Gaussian standing wave. *Opt. Rev.* **22**, 157–161 (2015). doi:10.1007/s10043-015-0027-3

41. E. Hebestreit, M. Frimmer, R. Reimann, L. Novotny, Sensing Static Forces with Free-Falling Nanoparticles. *Phys. Rev. Lett.* **121**, 063602 (2018). doi:10.1103/PhysRevLett.121.063602 Medline